4304 *Chem. Mater.* **2010,** *22,* 4304–4311
DOI:10.1021/cm100956k

CHEMISTRY OF MATERIALS
Article

Indifference of Superconductivity and Magnetism to Size-Mismatched Cations in the Layered Iron Arsenides $Ba_{1-x}Na_xFe_2As_2$

Raquel Cortes-Gil,[†] Dinah R. Parker,[†] Michael J. Pitcher,[‡] Joke Hadermann,[‡] and Simon J. Clarke*,[†]

[†]*Department of Chemistry, University of Oxford, Inorganic Chemistry Laboratory, South Parks Road, Oxford OX1 3QR, U.K., and* [‡]*EMAT, University of Antwerp, Groenenborgerlaan 171, 2020 Antwerp, Belgium*

Received April 6, 2010. Revised Manuscript Received June 17, 2010

The evolution of the structure, magnetic ordering, and superconductivity in the series $Ba_{1-x}Na_xFe_2As_2$ is reported up to the limiting Na-rich composition with $x = 0.6$; the more Na-rich compositions are unstable at high temperatures with respect to competing phases. The magnetic and superconducting behaviors of the $Ba_{1-x}Na_xFe_2As_2$ members are similar to those of the better-investigated $Ba_{1-x}K_xFe_2As_2$ analogues. This is evidently a consequence of the quantitatively similar evolution of the structure of the FeAs layers in the two series. In $Ba_{1-x}Na_xFe_2As_2$ antiferromagnetic order and an associated structural distortion are evident for $x \leq 0.35$ and superconductivity is evident when x exceeds 0.2. For $0.4 \leq x \leq 0.6$ bulk superconductivity is evident, and the long-range antiferromagnetically ordered state is completely suppressed. The maximum T_c in the $Ba_{1-x}Na_xFe_2As_2$ series, as judged by the onset of diamagnetism, is 34 K in $Ba_{0.6}Na_{0.4}Fe_2As_2$. Despite the large mis-match in sizes between the two electropositive cations which separate the FeAs layers, there is no evidence for ordering of these cations on the length scale probed by electron diffraction.

Introduction

The recent discovery of superconductivity at 26 K in $LaFeAsO_{1-x}F_x$[1] has generated enormous interest, and subsequent investigations have led to the discovery of the first non copper-oxide superconductors with critical temperatures (T_c) exceeding 50 K. Iron arsenides represent a further class of high-T_c superconductors,[2] in which superconductivity occurs in compounds with layered structures and in which superconductivity lies in close proximity to antiferromagnetic order. Several studies suggest that superconductivity in these new compounds is non-BCS-like[3,4] and may be intimately related with magnetic fluctuations.[5,6] However, the details of the origin of superconductivity in these phases is still under intense debate.

LaFeAsO with the tetragonal ZrCuSiAs-type structure[7] contains cationic fluorite-type LaO layers alternating with antifluorite-type anionic FeAs layers. In the literature on these superconductors, compounds with this structure are often referred to as the "1111" series. LaFeAsO is a semimetal and exhibits Pauli paramagnetism with an anomaly in the magnetic susceptibility and specific heat at 135−140 K.[5,6] This transition is accompanied by a reduction of the lattice symmetry from tetragonal to orthorhombic around 150 K.[8] Somewhat below this structural transition antiferromagnetic long-range order sets in with small magnetic moments ($\sim 0.4\ \mu_B$) localized on the Fe atoms.[9] Changing the electron count within the FeAs layers by means of partial oxidation (hole doping)[10] or reduction (electron doping)[1,11] suppresses the antiferromagnetic long-range order and the structural phase transition, and the tetragonal phase becomes superconducting. Hence, the competition between superconductivity and antiferromagnetism in LaFeAsO derivatives is highly sensitive to the electron count in the FeAs layers. The precise superconducting properties appear also to be sensitive to the crystal structures: Lee et al. have observed that, assuming the optimal electron count, the highest values of T_c are obtained when

*To whom correspondence should be addressed. E-mail: simon.clarke@chem.ox.ac.uk. Fax: +44 1865 272690. Phone: +44 1865 272600.

(1) Kamihara, Y.; Watanabe, T.; Hirano, M.; Hosono, H. *J. Am. Chem. Soc.* **2008**, *130*, 3296.
(2) Johrendt, D.; Pöttgen, R. *Angew. Chem.* **2008**, *120*, 4860. Johrendt, D.; Pöttgen, R. *Angew. Chem., Int. Ed.* **2008**, *47*, 4782.
(3) Nakai, Y.; Ishida, K.; Kamihara, Y.; Hirano, M.; Hosono, H. *J. Phys. Soc. Jpn.* **2008**, *77*, 073701.
(4) Mazin, I. I.; Singh, D. J.; Johannes, M. D.; Du, M. H. *Phys. Rev. Lett.* **2008**, *101*, 057003.
(5) Dong, J.; Zhang, H. J.; Xu, G.; Li, Z.; Li, G.; Hu, W. Z.; Wu, D.; Chen, G. F.; Dai, X.; Luo, J. L.; Fang, Z.; Wang, N. *Europhys. Lett.* **2008**, *83*, 27006.
(6) Chen, G. F.; Li, Z.; Wu, D.; Li, G.; Hu, W. Z.; Dong, J.; Zheng, P.; Luo, J. L.; Wang, N. L. *Phys. Rev. Lett.* **2008**, *100*, 247002.
(7) Johnson, V.; Jeitschko, W. *J. Solid State Chem.* **1974**, *11*, 161.
(8) Nomura, T.; Kim, S. W.; Kamihara, Y.; Hirano, M.; Sushko, P. V.; Kato, K.; Takata, M.; Shluger, A. L.; Hosono, H. *Supercond. Sci. Technol.* **2008**, *21*, 125028.
(9) De la Cruz, C.; Huang, Q.; Lynn, J. W.; Li, J.; Ratcliff, W., II; Zarestky, J. L.; Mook, H. A.; Chen, G. F.; Luo, J. L.; Wang, N. L.; Dai, P. *Nature* **2008**, *453*, 899.
(10) Wen, H.-H.; Mu, G.; Fang, L.; Yang, H.; Zhu, X. *Europhys. Lett.* **2008**, *82*, 17009.
(11) Che, G.-C.; Dong, X.-L.; Yang, J.; Lu, W.; Yi, W.; Shen, X.-L.; Li, Z.-C.; Sun, L.-L.; Zhou, F.; Zhao, Z.-X. *Europhys. Lett.* **2008**, *83*, 17002.

Published on Web 07/02/2010

the $FeAs_4$ tetrahedra are close to regular.[12,13] Evidently the competition between the instability which leads to magnetic order in these itinerant antiferromagnets and the instability which leads to superconductivity is finely balanced and depends on the details of the Fermi surface which are dictated by the crystal structure and the electron count, and also depends on the disorder which inevitably accompanies chemical substitution.

$BaFe_2As_2$ with the $ThCr_2Si_2$ structure[14] is the archetypal representative of the "122" type pnictide superconductors; FeAs layers structurally similar to, and isoelectronic with, those in LaFeAsO, exhibited very similar magnetic susceptibility, conductivity, and heat capacity to LaFeAsO.[15] The only significant difference is that the structural transition and the transition to the magnetically ordered state are coincident at 140 K. In the course of this phase transition, the tetragonal symmetry of the $ThCr_2Si_2$-type structure (space group $I4/mmm$) changes into the orthorhombic β-$SrRh_2As_2$-type (space group $Fmmm$)[16] and long-range antiferromagnetic ordering appears.[15] Hole doping in $BaFe_2As_2$ to change the electron count of the FeAs layers suppresses the structural and magnetic transitions and induces superconductivity. The maximum value of T_c of 38 K was obtained in $Ba_{0.6}K_{0.4}Fe_2As_2$,[17], but superconductivity persists over a wide range of electron counts and only the very Ba-rich members of the $Ba_{1-x}K_xFe_2As_2$ solid solution do not superconduct. Alternatively the superconducting state can be stabilized by substituting Fe by Co within the arsenide layer as in the well-studied $Ba(Fe_{1-x}Co_x)_2As_2$.[18] The suppression of antiferromagnetic order and the emergence of superconductivity can furthermore be accomplished by the application of an external hydrostatic pressure[19,20] or by modifying the band structure by making substitutions on the pnictide site in $BaFe_2(As_{1-x}P_x)_2$.[21,22]

Superconductivity appears to be ubiquitous in compounds containing FeAs (and sometimes FeP or FeSe) antifluorite-type layers. $SrFe_2As_2$,[23−25] $CaFe_2As_2$,[26,27] and $EuFe_2As_2$[28,29] are further members of the 122-series in which superconductivity may be realized by appropriate doping. The 122 systems are most amenable to crystal growth for physical property measurements, and the systems $Ba_{1-x}K_xFe_2As_2$[30] and $Ba(Fe_{1-x}Co_x)_2As_2$[31] have received extensive attention. The evolution of the crystal structure, phase transition, and superconductivity in the solid solution $Ba_{1-x}K_xFe_2As_2$ ($0 \le x \le 1$) have been reported by Rotter et al.[30], and Nandi et al.[31] have demonstrated how the suppression of antiferromagnetic order and the orthorhombic distortion in $Ba(Fe_{1-x}Co_x)_2As_2$ are coupled to the emergence of superconductivity. In general doping on the alkaline earth site has been restricted to using alkali metals with similar ionic radius to the alkaline earth metals in the parent phase. The $Ba_{1-x}K_xFe_2As_2$ solid solution occurs for $0 \le x \le 1$[32] because of the similar ionic radii of Ba^{2+} and K^{+}[33] and the tolerance of the tetragonal $ThCr_2Si_2$-type structure to electron count. Substitution of the alkaline earth by Na^+ has been reported in $CaFe_2As_2$ and $EuFe_2As_2$;[26,27,29] however, the full solid solution cannot be obtained at the high temperatures used in synthesis: the square prismatic site is too large for Na^+, and although $NaFe_2As_2$ may be formed at low temperatures,[34] it is metastable with respect to the formation of NaFeAs[35] and FeAs. In NaFeAs[35,36] and LiFeAs[37−39] with the anti-PbFCl structure the smaller alkali cations are in a 5-coordinate square pyramidal site.

In spite of the great difference in the ionic radii of Ba^{2+} and Na^+ (for comparison the values for sites 8-coordinate by oxide are (1.42 Å and 1.16 Å respectively)),[33] we have stabilized $Ba_{1-x}Na_xFe_2As_2$ over a wide compositional range ($0 \le x \le 0.6$). These compounds and the evolution

(12) Lee, C. H.; Iyo, A.; Eisaki, H.; Kito, H.; Fernandez-Diaz, M. T.; Ito, T.; Kihou, K.; Matsuhata, H.; Braden, M.; Yamada, K. *J. Phys. Soc. Jpn.* **2008**, *77*, 083704.
(13) Mizuguchi, Y.; Hara, Y.; Deguchi, K.; Tsuda, S.; Yamaguchi, T.; Takeda, K.; Kotegawa, H.; Tou, H.; Takano, Y. *Superconductor Science and Technology* **2010**, *23*, 054013.
(14) Pfisterer, M.; Nagorsen, G. *Z. Naturforsch. B* **1980**, *35*, 703.
(15) Rotter, M.; Tegel, M.; Joherendt, D.; Schellenberg, I.; Hermes, W.; Pöttgen, R. *Phys. Rev. B* **2008**, *78*, 020503(R).
(16) Hellmann, A.; Löhken, A.; Wurth, A.; Mewis, A. *Z. Naturforsch. B* **2007**, *62*, 155.
(17) Rotter, M.; Tegel, M.; Joherendt, D. *Phys. Rev. Lett.* **2008**, *101*, 107006.
(18) Sefat, A. S.; Jin, R.; McGuire, M. A.; Sales, B. C.; Singh, D. J.; Mandrus, D. *Phys. Rev. Lett.* **2008**, *101*, 117004.
(19) Park, T.; Park, E.; Lee, H.; Klimczuk, T.; Bauer, E. D.; Ronning, F.; Thompson, J. D. *J. Phys.: Condens. Matter* **2008**, *20*, 322204.
(20) Alireza, P. L.; Gillett, J.; Ko, Y. T. C.; Sebastian, S. E.; Lonzarich, G. G. *J. Phys.: Condens. Matter* **2009**, *21*, 012208.
(21) Jiang, S.; Xing, H.; Xuan, G.; Wang, C.; Ren, Z.; Feng., C.; Dai, J.; Xu., Z.; Cao, G. *J. Phys.: Condens. Matter* **2009**, *21*, 382203.
(22) Kasahara, S.; Shibauchi, T.; Hashimoto, K.; Ikada, K.; Tonegawa, S.; Okazaki, R.; Shishido, H.; Ikeda, H.; Takeya, H.; Hirata, K.; Terashima, T.; Matsuda, Y. *Phys. Rev. B* **2010**, *81*, 184519.
(23) Chen, G. F.; Li, Z.; Li, G.; Hu, W. Z.; Dong, J.; Zhou, J.; Zhang, X. D.; Zheng, P.; Wang, N. L.; Luo, J. L. *Chin. Phys. Lett.* **2008**, *25*, 3403.
(24) Chen, G. F.; Li, Z.; Dong, J.; Li, G.; Hu, W. Z.; Zhang, X. D.; Song, X. H.; Zheng, P.; Wang, N. L.; Luo, J. L. *Phys. Rev. B* **2008**, *78*, 224512.
(25) Sasmal, K.; Lv, B.; Lorenz, B.; Guloy, A. M.; Cheng, F.; Xue, Y.-Y; Chu, C.-W *Phys. Rev. Lett.* **2008**, *101*, 107007.
(26) Wu, G.; Chen, H.; Wu, T.; Xie, Y. L.; Yan, Y. J.; Liu, R. H.; Wang, X. F.; Ying, J. J.; Chen, X. H. *J. Phys.: Condens. Matter* **2008**, *20*, 422201.
(27) Shirage, P. M.; Miyazawa, K.; Kito, H.; Eisaki, H.; Iyo, A. *Appl. Phys. Express* **2008**, *1*, 081702.
(28) Jeevan, H. S.; Hossain, Z.; Kasinathan, D.; Rosner, H.; Geibel, C.; Gegenwart, P. *Phys. Rev. B* **2008**, *78*, 092406.
(29) Qi, Y.; Gao, Z.; Wang, L.; Wang, D.; Zhang, X.; Ma, Y. *New J. Phys.* **2008**, *10*, 123003.
(30) Rotter, M.; Pangerl, M.; Tegel, M.; Joherendt, D. *Angew. Chem., Int. Ed.* **2008**, *47*, 7949.
(31) Nandi, S.; Kim, M. G.; Kreyssig, A.; Fernandes, R. M.; Pratt, D. K.; Thaler, A.; Ni, N.; Bud'ko, S. L.; Canfield, P. C.; Schmalian, J.; McQueeney, R. J.; Goldman, A. I. *Phys. Rev. Lett.* **2010**, *104*, 057006.
(32) Rozsa, S.; Schuster, H.-U. *Z. Naturforsch. B* **1981**, *36*, 1668.
(33) Shannon, R. D.; Prewitt, C. T. *Acta Crystallogr., Sect. B* **1969**, *25*, 925.
(34) Gooch, M.; Lv, B.; Sasmal, K.; Tapp, J. H.; Tang, Z. J.; Guloy, A. M.; Lorenz, B.; Chu, C. W. *Physica C* **2009**, in press; DOI: 10.1016/j.physc.2009.10.096.
(35) Parker, D. R.; Pitcher, M. J.; Baker, P. J.; Franke, I.; Lancaster, T.; Blundell, S. J.; Clarke, S. J. *Chem. Commun.* **2009**, *16*, 2189.
(36) Parker, D. R.; Smith, M. J. P.; Lancaster, T.; Steele, A. J.; Franke, I.; Baker, P. J.; Pratt, F. L.; Pitcher, M. J.; Blundell, S. J.; Clarke, S. J. *Phys. Rev. Lett.* **2010**, *104*, 057007.
(37) Pitcher, M. J.; Parker, D. R.; Adamson, P.; Herkelrath, S. J. C.; Boothroyd, A. T.; Ibberson, R. M.; Brunelli, M.; Clarke, S. J. *Chem. Commun.* **2008**, *45*, 5918.
(38) Tapp, J. H.; Tang, Z.; Lv, B.; Sasmal, K.; Lorenz, B.; Chu, P. C. W.; Guloy, A. M. *Phys. Rev.B.* **2008**, *78*, 060505(R).
(39) Wang, X. C.; Liu, Q. Q.; Lv, Y. X.; Gao, W. B.; Yang, L. X.; Yu, R. C.; Li, F. Y.; Jin, C. Q. *Sol. State Commun.* **2008**, *148*, 538.

from the antiferromagnetic semimetal $BaFe_2As_2$ to superconducting hole-doped phases are described in this article.

Experimental Section

All manipulations were carried out in an argon-filled glovebox. $Ba_{1-x}Na_xFe_2As_2$ ($0 \le x \le 0.6$) were synthesized by heating stoichiometric mixtures of the elements. Ba (rods, Aldrich 99%) was purified by sublimation onto a copper coldfinger under high vacuum at 950 °C prior to use. Na lump (BDH 99.9%) and Fe powder (ALFA 99.998%) were used as received, and As pieces (ALFA 99.9999%) were pulverized prior to use. Fe and As were ground together and placed on top of the appropriate amounts of the electropositive metals inside 9 mm diameter Nb tubes which were then welded closed under 1 atm of argon in an arc furnace and heated in protective evacuated silica tubes. The mixtures were heated at 1 °C min^{-1} to 800 °C. This temperature was maintained for 3 days, and the reaction vessels were then cooled rapidly to room temperature by removing them from the hot furnace. After homogenization in an agate mortar inside the glovebox, the products were annealed at 900 °C for 30 h, and once again, cooled rapidly to room temperature. For $x \ge 0.5$ the powders were pressed into 13 mm diameter pellets prior to the annealing step. The compounds are black with metallic luster and are stable in air and moisture for at least several weeks.

Powder X-ray diffraction (PXRD) measurements were carried out using a PANalytical X′pert PRO diffractometer operating with Cu$K_{\alpha 1}$ radiation in Bragg−Brentano geometry at room temperature with the sample mounted on a silicon wafer. Crystal structures were refined by the Rietveld method using the GSAS software package.[40] Neutron powder diffraction (NPD) measurements at room and low temperature were performed using the diffractometers D2B (ILL, Grenoble), POLARIS and OSIRIS (ISIS, U.K.) with the samples contained in thin-walled vanadium cylinders.

Selected area electron diffraction (SAED) measurements were performed on Philips CM20 and Tecnai G2 transmission electron microscopes. High angle annular dark field stem images (HAADF-STEM) were taken on the Tecnai G2 instrument.

To characterize the magnetic and superconducting properties, zero-field-cooled (ZFC) and field-cooled (FC) magnetization measurements were performed from 2 to 300 K in a measuring field of 50 Oe using a SQUID magnetometer (Quantum Design, MPMS-XL).

Results and Discussion

Samples of $Ba_{1-x}Na_xFe_2As_2$ with $x \le 0.6$ appeared single phase according to laboratory PXRD measurements. Attempts to prepare materials richer in Na resulted in the formation of impurity phases. Reactions intended to produce $Ba_{0.38}Na_{0.62}Fe_2As_2$ and $Ba_{0.36}Na_{0.64}Fe_2As_2$ yielded $Ba_{1-x}Na_xFe_2As_2$ phases together with a NaFeAs impurity, and samples even richer in Na (i.e., $Ba_{0.3}Na_{0.7}Fe_2As_2$ and $Ba_{0.2}Na_{0.8}Fe_2As_2$) produced additional impurities of Fe_2As and Na_3As.

Room Temperature Crystal Structures. The trends in the crystal structures of the compounds $Ba_{1-x}Na_xFe_2As_2$ were determined by Rietveld refinements against PXRD and NPD data. All compositions crystallize at room temperature in the tetragonal $ThCr_2Si_2$-type structure with space group $I4/mmm$. Figure 1 and Table 1 show the variation of the room temperature lattice parameters with sodium doping from laboratory PXRD data. The lattice parameters a and c vary approximately linearly with the sodium concentration in the range $0 \le x \le 0.4$. In this compositional range the basal a axis decreases with increasing x while the c axis perpendicular to the FeAs layers increases. This behavior of the lattice parameters is qualitatively similar to that displayed by $Ba_{1-x}K_xFe_2As_2$ over the entire compositional range $0 \le x \le 1$.[30] The behavior of the basal lattice parameter (i.e., $\sqrt{2} \times$ Fe−Fe) is furthermore *quantitatively* similar in the $Ba_{1-x}K_xFe_2As_2$ and $Ba_{1-x}Na_xFe_2As_2$ series. Because of the smaller radius of Na^+ compared with K^+ the increase in c in the $Ba_{1-x}Na_xFe_2As_2$ series is less rapid with x than in the $Ba_{1-x}K_xFe_2As_2$ series up to $x = 0.4$.

For $x > 0.4$ in $Ba_{1-x}Na_xFe_2As_2$ the basal lattice parameter continues to shrink, and the c parameter also shrinks as the Na/Ba ratio exceeds 1 at $x = 0.5$. Given these trends in the lattice parameters, the unit cell volume decreases rapidly with x as the sodium-rich limit at $x = 0.6$ is approached. Overall the cell volume decreases by 4% in the range $0 \le x \le 0.6$. In $Ba_{1-x}K_xFe_2As_2$ the cell volume is almost constant over the entire compositional range because the contraction in a compensates the increase in c. In none of the powder diffraction patterns

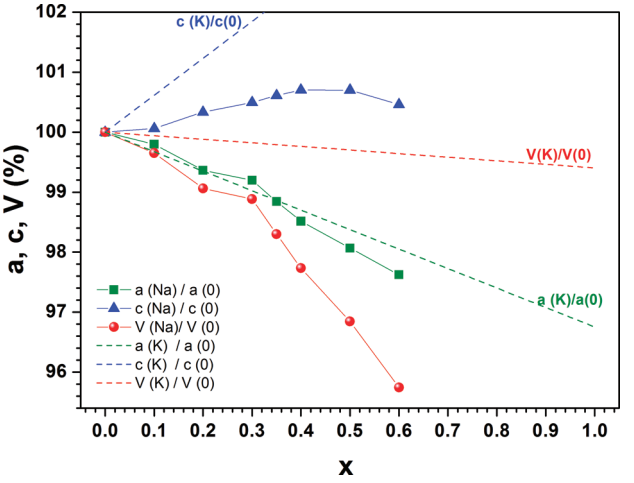

Figure 1. Evolution at room temperature of the lattice parameters and unit cell volume of $Ba_{1-x}Na_xFe_2As_2$ ($0 \le x \le 0.6$) as a function of x, compared with the corresponding evolution in $Ba_{1-x}K_xFe_2As_2$ ($0 \le x \le 1$) (ref 30). Values are given as percentages of the values in $BaFe_2As_2$.

Table 1. Lattice Parameters of $Ba_{1-x}Na_xFe_2As_2$ ($0 \le x \le 0.6$) from PXRD Data at Room Temperature and from NPD at 5 K

	300 K		5 K		
x	a (Å)	c (Å)	a (Å)	b (Å)	c (Å)
0	3.96513	13.02689	5.61460	5.57125	12.94530
0.1	3.957064(6)	13.03490(3)	5.6074(1)	5.5646(1)	12.9479(3)
0.2	3.939903(9)	13.07026(4)	5.5804(1)	5.5406(1)	12.9517(3)
0.3	3.93327(1)	13.09115(5)	5.5744(1)	5.5385(1)	12.9787(3)
0.35	3.919322(9)	13.10666(4)	5.5396(1)	5.5278(1)	12.9914(2)
0.4	3.90625(1)	13.11847(5)	3.89584(8)		12.9940(3)
0.5	3.88846(5)	13.11820(2)	not measured		
0.6	3.87090(2)	13.08699(8)	not measured		

(40) Larson, A. C.; Dreele, R. B. *General Structure Analysis System*; Los Alamos National Laboratory Report LAUR; Los Alamos National Laboratory: Los Alamos, NM, 2004; pp 86−748.

were there any superstructure reflections to indicate ordering of the two differently sized cations on the length scale probed by X-ray or neutron diffraction methods. The possibility of ordering of the electropositive cations was probed using electron diffraction. The SAED patterns along the directions [100], [110], and [001] of $Ba_{0.6}Na_{0.4}Fe_2As_2$ are shown in Figure 2 and show only reflections belonging to the *I*4/*mmm* lattice determined by XRD. Nor was there any evidence for diffuse scattering in these diffraction patterns. The absence of certain types of local order (e.g., ordering into Na-rich and Ba-rich columns) is also supported by HAADF-STEM images; a representative image along [100] is shown in Figure 3. In these images the brightness of a projected column is related to its average atomic number along the column. Thus Ba and Na columns should give respectively bright and low intensity dots. On the HAADF-STEM images overall all dots at the Na/Ba position have similar brightness, with no sign of order between the cations.

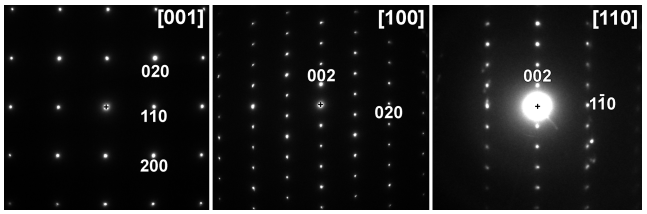

Figure 2. SAED patterns along [100], [110], and [001] of $Ba_{0.6}Na_{0.4}Fe_2As_2$.

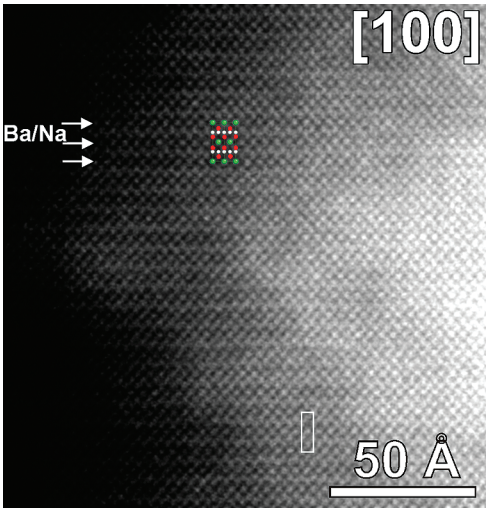

Figure 3. HAADF-STEM image along [100]. The model is put over a small area of the image to indicate the correspondence of the different dots to specific projected atom columns. Green spheres are Ba/Na, white are Fe, red are As. The white arrows indicate the Ba/Na layers. The size of one unit cell is indicated by a white rectangle.

The trends in the Fe−Fe bond length follow those in the *a* lattice parameter because Fe−Fe = $a/\sqrt{2}$. This and other structural parameters at room temperature obtained from NPD measurements are compiled in Tables 2−4. The Fe−Fe distance and the As−Fe−As bond angles are the parameters which change most significantly with hole doping (Figures 4a and 4b). The Fe−Fe distance decreases approximately linearly with increasing sodium content while the change in Fe−As bond length is almost an order of magnitude smaller than the change in the Fe−Fe distance. The $FeAs_4$ tetrahedra therefore change from being slightly compressed along the *c* axis in $BaFe_2As_2$ to being slightly compressed in the basal plane in $Ba_{0.4}Na_{0.6}Fe_2As_2$ relative to a regular tetrahedron. The increase in the compression of the $FeAs_4$ tetrahedra in the basal direction coupled with the fact that at small Na contents, the interplanar As−As distance (Figure 4c) is almost invariant with *x* in $Ba_{1-x}Na_xFe_2As_2$ accounts for the initial increase in the length of the *c* axis (Figure 1). At higher Na contents ($x > 0.3$) both the basal lattice parameter and the interplanar As−As distance decrease at similar rates (by 1.5% in the range $0.3 \leq x \leq 0.6$) as the average (Ba,Na)−As distance decreases sharply (Figure 4d). This decrease in the interplanar As−As distance for $x > 0.3$ which becomes increasingly rapid with *x* as *x* increases means that the *c* axis length decreases as the Na-rich limit is approached. Representative NPD patterns at room temperature and at 200 K are shown for $Ba_{0.9}Na_{0.1}Fe_2As_2$ in Figures 5a and 5b.

Low Temperature Crystal Structures. PND patterns collected at 5 K (Figure 5c) show that like in $BaFe_2As_2$, several reflections split at low temperature in the $Ba_{1-x}Na_xFe_2As_2$ phases with $x < 0.4$. The patterns at 5 K were

Table 3. Bond Distances for $Ba_{1-x}Na_xFe_2As_2$ ($0 \leq x \leq 0.6$) from NPD Data at Room Temperature

x	Fe−Fe (Å)	Fe−As (Å)	Ba/Na−As (Å)	As−As (Å)
0[a,d]	2.798	2.395	3.378	3.786
0.1[b,d]	2.79718(2)	2.4011(2)	3.3793(2)	3.793(6)
0.2[c,d]	2.78334(3)	2.3973(9)	3.3679(9)	3.792(3)
0.3[c,d]	2.77845(6)	2.400(1)	3.361(1)	3.784(4)
0.35[b,d]	2.77073(3)	2.3989(2)	3.3544(2)	3.782(6)
0.4[c,d]	2.75858(3)	2.3967(7)	3.3403(7)	3.767(2)
0.5[b,d]	2.75047(2)	2.3954(2)	3.3324(2)	3.763(1)
0.6[c,d]	2.73395(4)	2.3919(9)	3.3064(8)	3.719(2)

[a] ref 42. [b] POLARIS (ISIS, UK). [c] D2B (ILL, France). [d] Space Group: *I*4/*mmm* (No.139). Ba,Na: 2*a* (0,0,0), Fe: 4*d* (1/2,0,1/4), As 4*e* (0,0,*z*).

Table 2. Refined Atomic Parameters for $Ba_{1-x}Na_xFe_2As_2$ ($0 \leq x \leq 0.6$) from NPD Data at Room Temperature

x	$10^4 \times$ (Ba/Na U_{iso}(Å^2))	$10^4 \times$ (Fe U_{iso} (Å^2))	As *z*	$10^4 \times$ As U_{iso} (Å^2)
0[a,d]	95(5)	57(6)	0.35405(8)	99(5)
0.1[b,d]	83(1)	64(1)	0.35447(2)	68(1)
0.2[c,d]	80(10)	84(4)	0.3548(1)	87(6)
0.3[c,d]	110(10)	77(5)	0.3554(2)	90(6)
0.35[b,d]	129(2)	81(1)	0.35567(3)	94(1)
0.4[c,d]	128(6)	65(3)	0.35627(9)	78(3)
0.5[b,d]	142(1)	76(1)	0.35659(3)	82(1)
0.6[c,d]	174(8)	69(3)	0.3577(1)	84(4)

[a] Ref 42. [b] POLARIS (ISIS, U.K.). [c] D2B (ILL, France). [d] Space Group: *I*4/*mmm* (No.139). Ba,Na: 2*a* (0,0,0), Fe: 4*d* (1/2,0,1/4), As 4*e* (0,0,*z*).

Table 4. Bond Angles for $Ba_{1-x}Na_xFe_2As_2$ ($0 \le x \le 0.6$) from NPD Data at Room Temperature

x	As−Fe−As (deg) × 2	As−Fe−As (deg) × 4	As−(Ba/Na)−As (deg) × 2	As−(Ba/Na)−As (deg) × 4
0[a,d]	111.411	108.510	111.847	71.703
0.1[b,d]	110.92(1)	108.750(6)	111.731(9)	71.647(4)
0.2[c,d]	110.37(6)	109.026(26)	111.47(4)	71.52(2)
0.3[c,d]	109.90(9)	109.26(5)	111.50(7)	71.53(3)
0.35[b,d]	109.51(1)	109.451(7)	111.38(1)	71.475(5)
0.4[c,d]	108.95(5)	109.731(23)	111.35(3)	71.46(2)
0.5[b,d]	108.57(1)	109.92(7)	111.25(1)	71.41(5)
0.6[c,d]	107.85(6)	110.29(3)	111.56(4)	71.56(2)

[a] Ref 42. [b] POLARIS (ISIS, U.K.). [c] D2B (ILL, France). [d] Space Group: *I*4/*mmm* (No.139). Ba,Na: 2*a* (0,0,0), Fe: 4*d* (1/2,0,1/4), As 4*e* (0,0,*z*).

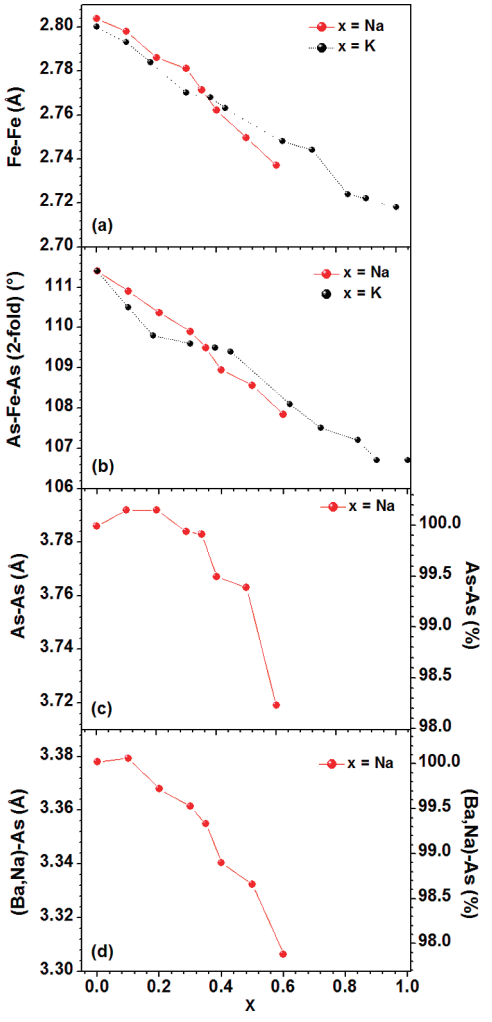

Figure 4. Variation of structural parameters at room temperature in $Ba_{1-x}Na_xFe_2As_2$ ($0 \le x \le 0.6$) as a function of x: (a) Fe−Fe bond length, (b) As−Fe−As angle, (c) As−As distance, and (d) (Ba,Na)−As bond length. Comparative data for $Ba_{1-x}K_xFe_2As_2$ data (ref 30) are shown.

indexed with an orthorhombic *F*-centered unit cell, and a structural model corresponding to the β-$SrRh_2As_2$-type was refined in the space group *Fmmm*. To delimit the composition range of the structural transition, we have studied the dependence of the (112) reflection of the tetragonal structure at low temperature with Na content (Figure 6). Peak splitting into the orthorhombic (022) and (202) reflections is well resolved at $x = 0.1$ and 0.2, and peak broadening is evident for $x = 0.3$. The highest resolution data collected on OSIRIS for the $x = 0.35$ sample (Figure 6d) shows a just-discernible peak broadening on cooling from

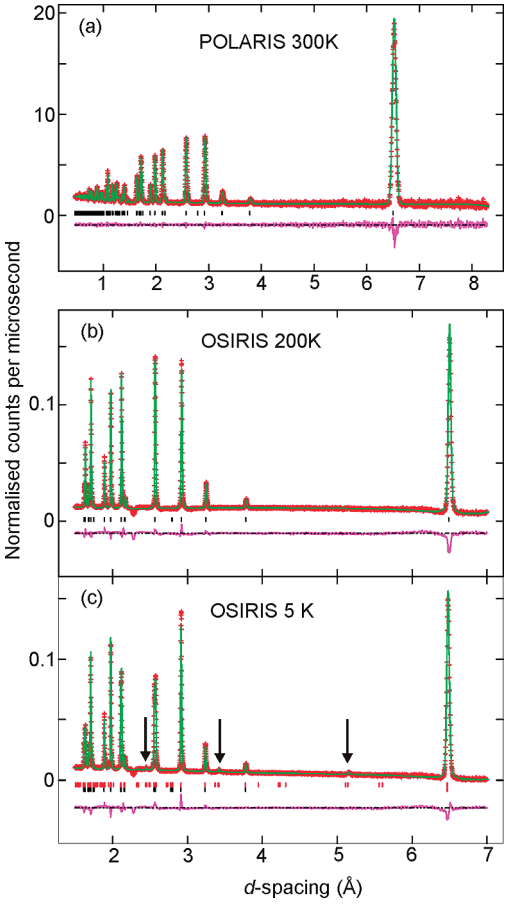

Figure 5. NPD pattern and Rietveld fit of $Ba_{0.9}Na_{0.1}Fe_2As_2$ at (a) 300 K, (b) 200 K, and (c) 5 K with magnetic Bragg peaks indicated.

200 to 5 K, but for the $x = 0.4$ sample (Figure 6e) the distortion is not evident at the resolution of the diffractometer. We conclude that there is evidence for an orthorhombic distortion up to $x = 0.35$, but for larger x contents the tetragonal $ThCr_2Si_2$-type structure in space group *I*4/*mmm* is retained at all temperatures. This is in agreement with the observation that the structural transition in $Ba_{1-x}K_xFe_2As_2$ is only evident for $x < 0.4$.[41] Table 1 and Figure 7 show the 5 K lattice parameters as a function of Na doping. The size of the orthorhombic distortion in $Ba_{1-x}Na_xFe_2As_2$ quantified as a/b-1 is shown in Figure 7c where it is compared with the distortion in $Ba_{1-x}K_xFe_2As_2$.

(41) Chen, H.; Ren, Y.; Qiu, Y.; Wei Bao, Liu, R. H.; Wu, G.; Wu, T.; Xie, Y. L.; Wang, X. F.; Huang, Q.; Chen, X. H. *Europhys. Lett.* **2009**, *85*, 17006.

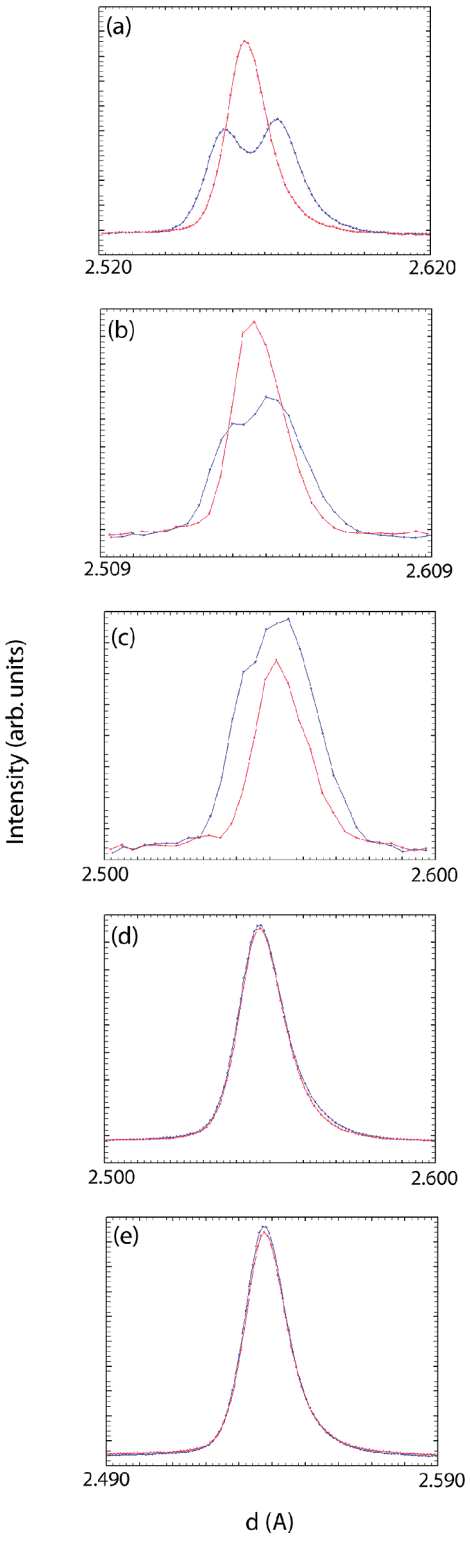

Figure 6. Comparison of the tetragonal (112)/orthorhombic (022)/(202) reflections at room temperature (red) and 5 K (blue) in $Ba_{1-x}Na_xFe_2As_2$: (a) $x = 0.1$ (OSIRIS), (b) $x = 0.2$ (D2B), (c) $x = 0.3$ (D2B), (d) $x = 0.35$ (OSIRIS), and (e) $x = 0.4$ (OSIRIS).

Magnetic Ordering. Bragg peaks due to antiferromagnetic ordering of moments located on Fe are evident in the 5 K neutron diffractogram for $x \leq 0.35$ (Figure 5c).

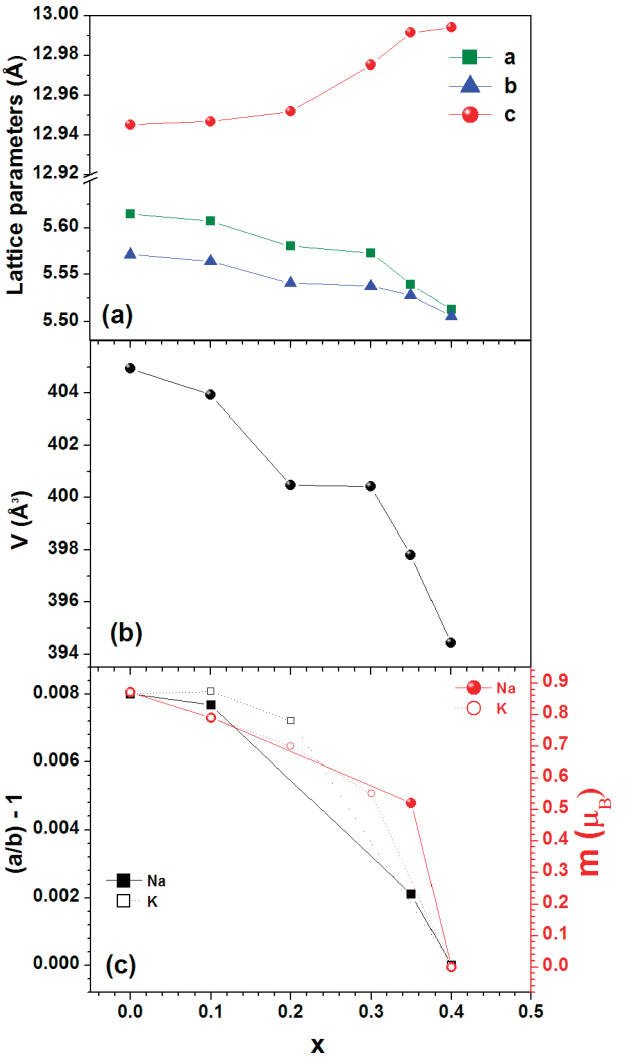

Figure 7. Variation of structural parameters in $Ba_{1-x}Na_xFe_2As_2$ ($0 \leq x \leq 0.4$) with x: (a) lattice parameters and (b) unit cell volume. Panel (c) shows the similar dependence of the orthorhombic distortion on ordered magnetic moment at 5 K in $Ba_{1-x}Na_xFe_2As_2$ ($0 \leq x \leq 0.6$) and $Ba_{1-x}K_xFe_2As_2$.[41]

In accordance with the reported magnetic structure of $BaFe_2As_2$ the Bragg peaks may be accounted for using a $\mathbf{q} = (101)_o$ magnetic wave vector,[42] with the Fe magnetic moments aligned antiferromagnetically along the a and c axes, and ferromagnetically along the shorter b axis in the orthorhombic unit cell as shown in Figure 8.

The undoped "parent" materials of the iron pnictide superconductors which formally have Fe in the +2 oxidation state generally adopt this magnetic structure and are itinerant antiferromagnets with small localized moments on the Fe atoms. The ordered magnetic moment at 5 K in $BaFe_2As_2$ is 0.87 μ_B per Fe.[42] This value decreases with the introduction of Na (Figure 7c) reaching a value of 0.52 μ_B in $Ba_{0.65}Na_{0.35}Fe_2As_2$. The ordered magnetic moment in $Ba_{0.65}Na_{0.35}Fe_2As_2$ is nevertheless higher than that in LaFeAsO, the parent of the 1111 iron arsenide superconductors (0.36 μ_B).[9] Like the evolution of the structure of the FeAs layer, the evolution of the size of the magnetic moment with composition is quantitatively similar in $Ba_{1-x}Na_xFe_2As_2$ and $Ba_{1-x}K_xFe_2As_2$[41] (Figure 7c).

(42) Huang, Q.; Qiu, Y.; Wey Bao, Green, M. A.; Lynn, J. W.; Gasparovic, Y. C.; Wu, T.; Wu, G.; Chen., X. H. *Phys. Rev. Lett.* **2008**, *101*, 257003.

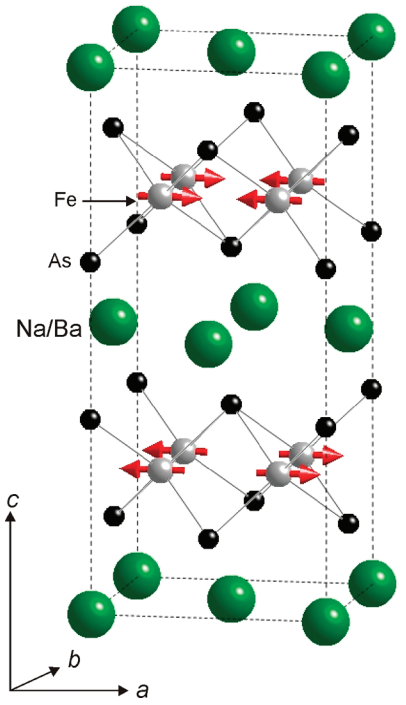

Figure 8. Magnetic and crystal structure of $Ba_{0.9}Na_{0.1}Fe_2As_2$. Fe magnetic moments are aligned antiferromagnetically along the *a* and *c* axes and ferromagnetically along the shorter *b* axis.

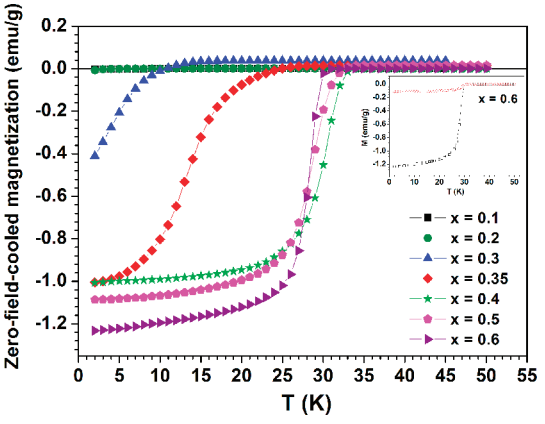

Figure 9. ZFC magnetization for $Ba_{1-x}Na_xFe_2As_2$ ($0 \le x \le 0.6$). The inset shows ZFC and FC data for $x = 0.6$.

Superconductivity. We have studied the evolution of superconductivity as a function of the Na concentration. Zero-field cooled (ZFC) and field cooled (FC) measurements were carried out in applied field of 50 Oe. Samples were all of a similar mass and shape, and no demagnetization correction was applied. For clarity, only ZFC measurements are shown in Figure 9, but for all the samples, both ZFC and FC susceptibilities exhibit diamagnetism (inset of Figure 9), and the hysteresis between them is typical for powder samples of these materials. Superconductivity emerges as x increases and bulk superconductivity is evident for $x \ge 0.4$ in $Ba_{1-x}Na_xFe_2As_2$ with the maximum value of 34 K (as judged by the onset of diamagnetism) found for $x = 0.4$ and decreasing only slightly up to the limiting composition of $x = 0.6$. The phase diagram in Figure 10 shows the superconducting critical temperature, as well as superconducting volume

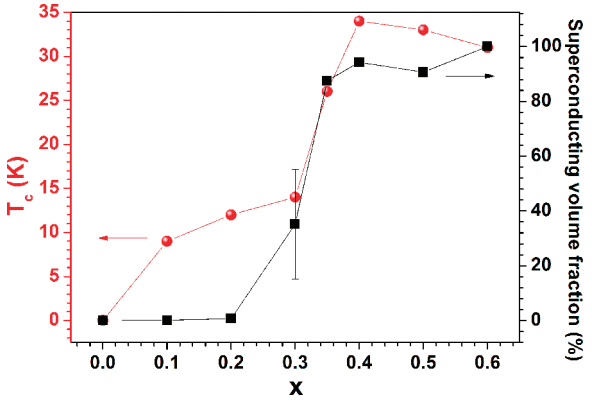

Figure 10. Phase diagram of $Ba_{1-x}Na_xFe_2As_2$ ($0 \le x \le 0.6$) with the critical temperature and superconducting volume fraction as a function of the sodium concentration. The large error bar in the superconducting volume fraction for the $x = 0.3$ sample reflects that the diamagnetism due to superconductivity has not saturated at 2 K.

fraction (estimated from the magnitude of ZFC signal at 5 K), as a function of the sodium concentration. Superconductivity is evident in the samples with $x = 0.3$ and 0.35 which also display magnetic Bragg peaks and show evidence for a low temperature orthorhombic distortion. However, in these cases the superconducting transition is much broader than in the more Na-rich materials with $x \ge 0.4$ which display no evidence for magnetic ordering.

Our work suggests that in the under-doped regime there may be separate regions of superconducting and magnetically ordered material: in the $x = 0.35$ sample there appears to be a significant superconducting volume fraction as judged by the magnitude of the diamagnetic susceptibility, but there are also magnetic Bragg peaks demonstrating that there are regions of long-range magnetically ordered material. X-ray and neutron diffraction methods are inherently a probe of the long-range average structure, so they are unable to distinguish between phase separation into regions smaller than several hundred nanometers or microscopic coexistence if the dimensions are smaller than several hundred nanometers. The question of whether phase separation is macroscopic or microscopic is a controversial one in these compounds. Our results are not inconsistent with the work of Park et al.[43] which reports electronic phase separation in slightly under-doped single crystal samples of $Ba_{1-x}K_xFe_2As_2$ (ref 43 does not specify the composition of the sample, but we presume it to be close to $Ba_{0.6}K_{0.4}Fe_2As_2$). The coexistence of magnetically ordered and nonmagnetic states in the same sample as probed using neutron scattering, muon-spin rotation spectroscopy, and magnetic force microscopy is explained by electronic phase separation into antiferromagnetic and superconducting regions on a scale of several tens of nanometers. NMR studies in polycrystalline $Ba_{1-x}K_xFe_2As_2$ samples synthesized by a high-pressure method suggested that the superconducting and magnetically ordered states do not coexist on the microscopic scale,

(43) Park, J. T.; Inosov, D. S.; Niedermayer, Ch.; Sun, G. L.; Haug, D.; Christensen, N. B.; Dinnebier, R.; Boris, A. V.; Drew, A. J.; Schulz, L.; Shapoval, T.; Wolff, U.; Neu, V.; Yang, X.; Lin, C. T.; Keimer, B.; Hinkov, V. *Phys. Rev. Lett.* **2009**, *102*, 117006.

but are rather present in separate regions.[44] However, in contrast with this report, Mössbauer spectroscopy on underdoped polycrystalline $Ba_{1-x}K_xFe_2As_2$ samples suggests the coexistence of magnetic ordering and superconductivity without mesoscopic phase separation.[45]

NMR studies on $Ba(Fe_{1-x}Co_x)_2As_2$ do show evidence for microscopic coexistence of the magnetic and superconducting states with each Fe atom involved in the competition between spin density wave magnetic order and superconductivity at low temperatures in $Ba(Fe_{1-x}Co_x)_2As_2$ with $x = 0.06$. In this system it has recently been shown that the strong competition between itinerant antiferromagnetism and superconductivity leads to suppression of the orthorhombic distortion in $Ba(Fe_{1-x}Co_x)_2As_2$ with x around 0.06 as it is cooled below T_c.[31]

In summary we report that the average structural changes in the FeAs layers of $Ba_{1-x}A_xFe_2As_2$ resulting from decreasing the electron count are independent of the average radius of the alkali metal cation A and the mismatch in radius between the alkaline earth and the alkali metal cations. This presumably accounts for the quantitative similarity between the evolution of the competing antiferromagnetic order and superconductivity in the $Ba_{1-x}Na_xFe_2As_2$ series and the well-studied $Ba_{1-x}K_xFe_2As_2$ series. The aversion of Na^+ to 8-coordination means that Ba may be only substituted by Na up to a limiting composition $Ba_{0.4}Na_{0.6}Fe_2As_2$. The similarity of the properties of the $Ba_{1-x}Na_xFe_2As_2$ and $Ba_{1-x}K_xFe_2As_2$ series for a given electron count supports the notion that the magnetism and superconductivity associated with the FeAs layers are dependent on the crystal structure and hence the electronic structure. However, the electronic behavior in these systems seems rather insensitive to the degree of disorder in the intervening layer of electropositive cations.

Acknowledgment. We are grateful to Dr. R. I. Smith and Dr. M. F. Telling for assistance at ISIS and Dr. E. Suard for assistance at ILL. We acknowledge STFC for the provision of beamtime. R.C.-G. acknowledges the support of a postdoctoral fellowship from *Ministerio de Educacion y Ciencia* of Spain.

Supporting Information Available: Tables of refined structural parameters at 5 K. This material is available free of charge via the Internet at http://pubs.acs.org.

(44) Fukazawa, H.; Yamazaki, T.; Kondo, K.; Kohori, Y.; Takeshita, N.; Shirage, P. M.; Kihou, K.; Miyazawa, K.; Kito, H.; Eisaki, H.; Iyo, A. *J. Phys. Soc. Jpn.* **2009**, *78*, 033704.
(45) Rotter, M.; Tegel, M.; Schellenberg, I.; Schappacher, F. M.; Pottgen, R.; Deisenhofer, J.; Gunther, A.; Schrettle, F.; Loidl, A.; Johrendt, D. *New J. Phys.* **2009**, *11*, 025014.